

**Arbeit zur Erlangung des akademischen Grades
Master of Science**

Working title

Jean-Marco Alameddine
geboren in Iserlohn

2019

Lehrstuhl für Experimentelle Physik V
Fakultät Physik
Technische Universität Dortmund

Erstgutachter: Prof. Dr. Dr. Wolfgang Rhode
Zweitgutachter: Prof. Dr. Zweitgutachter
Abgabedatum: 18. Dezember 2019

Kurzfassung

Hier steht eine Kurzfassung der Arbeit in deutscher Sprache inklusive der Zusammenfassung der Ergebnisse. Zusammen mit der englischen Zusammenfassung muss sie auf diese Seite passen.

Abstract

The abstract is a short summary of the thesis in English, together with the German summary it has to fit on this page.

Contents

1	Introduction	1
2	Theory	2
2.1	The lepton propagator PROPOSAL	2
3	Integration of rare processes	13
3.1	Muon pair production	13
3.2	Weak interaction of charged leptons	20
4	Propagation of electromagnetic showers	25
A	Anhang	26
	Bibliography	27

1 Introduction

2 Theory

2.1 The lepton propagator PROPOSAL

PROPOSAL (**P**ropagator with **O**ptimal **P**recision and **O**ptimized **A**speed for **A**ll **L**eptons) is a Monte Carlo simulation library capable of simulating the interactions of high energy leptons. The original program called MMC (**M**uon **M**onte **C**arlo) has been written in the programming language Java focusing on a precise but also fast muon and tau propagation [2]. On this basis, MMC has been rewritten within a dissertation to create the C++ library PROPOSAL [8]. To allow for a more universal use of the program, PROPOSAL can be used in Python through a wrapper as well. More modern programming concepts such as polymorphism and a modular code structure were introduced in a recent update of PROPOSAL [5].

The current version of the code is publicly available on GitHub¹ and can be used under the terms of a modified LGPL license. Examples of applications are the neutrino observatories IceCube and RNO who use PROPOSAL as a part of their simulation chain.

2.1.1 Calculation of energy losses

Energy losses of particles form the basis for the propagation algorithm in PROPOSAL. Assuming a particle with an initial energy E_i , an energy loss is described by its absolute value

$$\nu = E_i \cdot v \quad (2.1)$$

where v describes the relative energy loss of the particle and $E_f = E_i - \nu$ the final particle energy. Processes causing energy losses and implemented in PROPOSAL are

- bremsstrahlung,
- ionization,
- photonuclear interactions and

¹<https://github.com/tudo-astroparticlephysics/PROPOSAL>

- pair production of an electron-positron pair.

Quantitatively, the interaction probability for a process is described by its cross section σ . To describe the process with respect to a specific variable in the final state, the cross section can be written in a differential form, for example $d\sigma/dv$.

In principle, this information could be used right away to sample energy losses from differential cross sections, which are treated as probability density functions, by using inverse sampling. However, this approach would cause two immediate problems: Firstly, the propagation process would be very time inefficient since small energy losses, especially below the energy threshold of a detector, would be sampled individually. Secondly, numerical problems will occur due to the nature of the bremsstrahlung interaction: Since photons are massless, the bremsstrahlung cross sections diverges for $v \rightarrow 0$, making inverse sampling over the whole parameter range impossible.

As a solution, PROPOSAL differentiates between continuous and stochastic energy losses. The energy cut parameter v_{cut} is defined as

$$v_{\text{cut}} = \min [e_{\text{cut}}/E, v'_{\text{cut}}] \quad (2.2)$$

with a relative energy cut v'_{cut} and an absolute energy cut e_{cut} . Energy losses with $v < v_{\text{cut}}$ are treated as continuous losses, energy losses with $v > v_{\text{cut}}$ are treated as stochastic losses. The definition in (2.2) ensures that losses above an absolute detector threshold e_{cut} are treated as stochastic even if their relative value is below v_{cut} .

The propagation algorithm in PROPOSAL consists of numerous propagation steps where each step consists of continuous losses and a stochastic loss, see section 2.1.2 for a detailed description. To perform one propagation step, it is therefore necessary to have a mathematical expression to sample the next stochastic loss.

Let E_i be the initial energy of a particle and

$$P(E_f \leq E \leq E_i) = - \int_{E_i}^{E_f} p(E) \, dE \quad (2.3)$$

a cumulative distribution function describing the probability for a stochastic loss at a particle energy $E \geq E_f$. With inverse sampling, this function can be used to sample the energy of the occurrence of the next stochastic loss.

To derive an expression for (2.3), the distance between the initial particle position x_i and the position of the stochastic loss x_f is discretized into sections of Δx . The

2 Theory

probability for a stochastic loss after a distance of $x_f - x_i$, without any stochastic losses in the interval (x_i, x_f) , can be described as

$$\begin{aligned}\Delta P(x_f) &= P(x_f + \Delta x) - P(x_f) \\ &= (1 - \sigma(x_i)\Delta x) \cdot (1 - \sigma(x_{i+1})\Delta x) \cdot \dots \cdot (1 - \sigma(x_{f-1})\Delta x) \cdot \sigma(x_f)\Delta x \\ &\approx \exp\left(-\sum_{j=i}^{f-1} \sigma(x_j)\Delta x_j\right) \cdot \sigma(x_f)\Delta x\end{aligned}$$

where σ describes the probability for a stochastic loss. Note that $\Delta x \ll 1$ was used in the last step. In a differential form, the relation can be written as

$$dP(x_f) = \exp\left(-\int_{x_i}^{x_f} \sigma(x) dx\right) \cdot \sigma(x_f) dx_f \quad (2.4)$$

To transfer the dependency on the location x to a dependency on the energy E , the relation

$$f(E) = -\frac{dE}{dx} = E \frac{N_A}{A} \int_{v_{\min}}^{v_{\text{cut}}} \frac{d\sigma}{dv} dv \quad (2.5)$$

is introduced. Here, $f(E)$ describes the continuous energy losses between two stochastic losses and is calculated by taking the average energy loss for all interactions below the energy cut v_{cut} .

Applying (2.5) on (2.4) yields

$$dP(E_f) = \exp\left(\int_{E_i}^{E_f} \frac{\sigma(E)}{f(E)} dE\right) \cdot \frac{\sigma(E_f)}{-f(E_f)} dE_f. \quad (2.6)$$

The cumulative distribution function is obtained by integrating over the probabilities in (2.6):

$$\begin{aligned}P(E_f \leq E \leq E_i) &= \int_{P(E_i)=0}^{P(E_f)} dP(E_f) \\ &= \int_{E_i}^{E_f} \exp\left(\int_{E_i}^{E'} \frac{\sigma(E)}{f(E)} dE\right) \cdot \frac{\sigma(E')}{-f(E')} dE'.\end{aligned} \quad (2.7)$$

The expression in (2.7) is simplified by using the substitution

$$u(E) = \int_{E_i}^E \frac{\sigma(E')}{f(E')} dE', \quad du = \frac{\sigma(E)}{f(E)} dE \quad (2.8)$$

where the fundamental theorem of calculus has been applied to obtain the expression for du .

It follows that

$$\begin{aligned}
 P(E_f \leq E \leq E_i) &= - \int_{E_i}^{E_f} \exp(u(E'_f)) \, du \\
 &= [\exp(u(E'_f))]_{E_i}^{E_f} \\
 &= \exp(u(E_f)) - \underbrace{\exp(u(E_i))}_{=0} \\
 &= \exp\left(\int_{E_i}^{E_f} \frac{\sigma(E)}{f(E)} \, dE\right).
 \end{aligned} \tag{2.9}$$

By replacing the probability P in (2.9) by a random number $\xi \in (0, 1]$ the energy integral

$$\int_{E_i}^{E_f} \frac{\sigma(E)}{-f(E)} \, dE = -\log \xi, \tag{2.10}$$

originally derived in [2], is obtained. By sampling ξ , (2.10) can be used to calculate the energy of the occurrence of the next stochastic loss.

2.1.2 Propagation algorithm

The task of the propagation algorithm of PROPOSAL is to simulate the properties of the secondary particles produced in interactions as well as the properties of the initial particle after each interaction. This includes information on the energy, position, direction and time of the propagated particle and the secondary particles.

On the technical note, the structure of the propagation process in PROPOSAL is determined by the concept of a "chain of responsibility". Part of this chain are the *Sector* objects and a *Propagator* object.

Each *Sector* is defined by its geometry, its medium, its energy cut settings and other sector-specific properties. The cut settings itself differentiate between various particle positions with respect to a predefined *Detector* geometry. By having sectors with varying characteristics the user has the possibility to appropriately model the simulation environment.

The *Propagator* object chooses which sector is responsible for the propagation of the particle at its current position. The assigned *Sector* then propagates the particle

within its borders and returns the propagated particle back to the *Propagator*. This process is repeated either until the propagated distance of the initial particle surpasses a preset maximal propagation distance d_{\max} or until the initial particle energy falls below a preset threshold energy e_{low} .

The following steps give a simplified overview of the propagation process within a *Sector*.

Energy of the occurrence of the next interaction

According to (2.10), the energy of the occurrence of the next stochastic energy loss is calculated using a random number ξ . If

$$\xi > \exp \left(\int_{E_i}^{e_{\text{low}}} \frac{\sigma(E)}{f(E)} dE \right) \quad (2.11)$$

the sampled energy where the next stochastic loss occurs would fall below the threshold energy e_{low} , in this case there is no stochastic loss.

Furthermore, based on the lifetime τ of the initial particle, an energy where the particle decays is sampled. Both energy values are compared and the higher energy value, together with its interaction type (stochastic loss or decay), are used for the next step².

Particle displacement

Given the initial energy E_i and the energy of the interaction E_f , the (straight-lined) displacement is calculated with the tracking integral

$$x_f = x_i - \int_{E_i}^{E_f} \frac{dE}{f(E)} \quad (2.12)$$

where $x_f - x_i$ describes the propagated distance. If the calculated propagated distance would exceed the distance to the sector border d , E_f is recalculated by setting $x_f = x_i + d$ in (2.12) and solving the integral equation for E_f . In this case, no interaction will occur at E_f .

The elapsed time is determined by the time integral

$$t_f = t_i + \int_{x_i}^{x_f} \frac{dx}{v(x)} = t_i - \int_{E_i}^{E_f} \frac{dE}{f(E)v(E)} \quad (2.13)$$

²If a decay is the next interaction, the step "Simulation of the stochastic energy loss" is replaced accordingly by a decay method.

2.1 The lepton propagator PROPOSAL

with the particle velocity $v(E)$, or alternatively using the approximation $v = c$ with

$$t_f = t_i + \frac{x_f - x_i}{c}. \quad (2.14)$$

Optionally, PROPOSAL can apply multiple scattering effects on the calculated displacement. This changes the position of the next stochastic loss by sampling a deflection angle as well as the new direction of the particle. Currently, three different parametrizations for multiple scattering can be used in PROPOSAL: A parametrization based on Molière's theory of multiple scattering as well as two parametrizations based on a gaussian-like approximation of the Molière theory by Highland, see [6] for a detailed description of the scattering processes used in PROPOSAL.

Continuous energy losses and continuous randomization

The energy loss between E_i and E_f is treated continuously according to (2.5), meaning that the particle energy is set to $E = E_f$. However, this can cause discontinuities in the energy spectrum as shown in figure 2.1

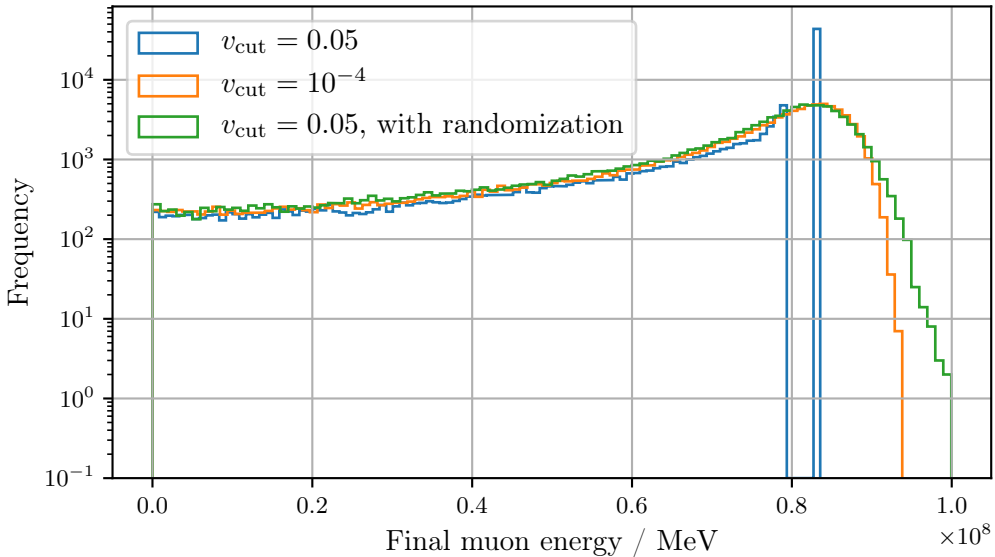


Figure 2.1: Energy spectrum of 10^5 muons with a starting energy of 10^8 MeV, propagated in 300 m of standard rock³. The spectrum shows the effects of an energy cut with or without continuous randomization.

³Standard rock means a material with $Z = 11$, $A = 22$ and a density of $\rho = 2.65 \text{ g/cm}^3$, see e.g. [11] for a detailed list of material properties.

2 Theory

For a sufficiently large v_{cut} , for example $v_{\text{cut}} = 0.05$ in figure 2.1, a peak in the final muon energy spectrum appears. This peak corresponds to all muons without any stochastic losses within the propagation distance. These particles all have the same final energy since no random numbers were effectively used to calculate their final energy, meaning that no fluctuations of the continuous losses are taken into account. Setting the energy cut to a significantly lower value, for example $v_{\text{cut}} = 10^{-4}$ in figure 2.1, eliminates the peak, however the runtime for the propagation is increased by at least an order of magnitude.

As a more time-efficient solution the option *continuous randomization* can be enabled in PROPOSAL. This applies fluctuations on the continuous loss energies sampled from a gaussian distribution. The mean of this distribution corresponds to $E_i - E_f$, the variance is calculated by

$$\langle \Delta(\Delta E)^2 \rangle = \int_{E_i}^{E_f} \frac{E^2}{-f(E)} \left\langle \frac{d^2 E}{dx^2} \right\rangle, \quad (2.15)$$

where the derivation of the variance follows similar steps to the derivation of (2.10), see [2] for a detailed derivation and description. The effects can be seen in figure 2.1, the energy spectrum becomes continuous and the running time behaves similarly to the running time for the propagation without continuous randomization.

Simulation of the stochastic energy loss

If the stochastic energy loss falls inside the sector and occurs before the initial particle decays, a stochastic loss at the energy E_f is sampled. The total stochastic cross section for the process i is calculated by

$$\sigma_{\text{stoch},i}(E_f) \propto \int_{v_{\text{cut}}}^{v_{\text{max}}} \frac{d\sigma_i(E_f)}{dv} dv. \quad (2.16)$$

Using a random number, the occurring process is calculated where the ratios of the process probabilities are represented by the ratios of the corresponding total stochastic cross sections. To calculate the relative size v of the stochastic loss, the integral equation

$$\frac{1}{\sigma_{\text{stoch},i}} \int_{v_{\text{cut}}}^v \frac{d\sigma_i}{dv} dv = \xi \quad (2.17)$$

is solved for v where $\xi \in [0, 1]$ is a random number and i the selected process.

The propagation routine is repeated by sampling the energy of the occurrence of the next interaction (i.e. the first step described here) until the particle has decayed, has reached the sector border or until its energy has reached the threshold energy e_{low} .

2.1.3 Muon propagation with PROPOSAL

At the end of the propagation process, PROPOSAL returns the properties of the produced secondary particles as well as the final properties of the initial particle or, if it did decay during propagation, its decay products. In this section the characteristic energy losses of muons are described, where ice is used exemplarily as a medium for all plots. The parametrizations for the interactions are always the default options in PROPOSAL, furthermore the Landau-Pomeranchuk-Migdal (LPM) effect for bremsstrahlung and pair production has been enabled.

In figure 2.2 the continuous energy losses of muons in ice, calculated according to (2.5), are shown. For this plot the energy cut has been set to $v_{\text{cut}} = v_{\text{max}}$, therefore the values shown correspond to the complete average energy losses of muons in ice. It can be seen that the average energy loss is quantitatively dominated by ionization for lower energies while e pair production, bremsstrahlung and photonuclear interactions become dominant for higher energies. Furthermore, it can clearly be seen that the parametrization

$$-\left\langle \frac{dE}{dx} \right\rangle \approx a(E) + b(E) \cdot E \quad (2.18)$$

Source for further description of the LPM effect?

of the average energy loss as a quasi-linear function is valid where $a(E)$ corresponds to energy losses due to ionization and $b(E)$ to energy losses due to e pair production, bremsstrahlung and photonuclear interactions. The parameters $a(E), b(E)$ vary only slightly with energy.

In figure 2.3 and 2.4 the stochastic losses for muons propagated in ice are shown, the energy cuts applied here are $e_{\text{cut}} = 500 \text{ MeV}$ and $v_{\text{cut}} = 0.05$ which corresponds to the energy cuts used in the analysis of the IceCube experiment. In both figures, the muons are propagated until they decay.

The histogram in figure 2.3 shows the energies of all secondary particles sorted by interaction type for 10^5 muons propagated with an initial energy of 10^8 MeV . Between about 10^3 MeV and 10^6 MeV the energy losses are dominated by e pair production, this dominance could for example be used to probe the e pair production cross section in this energy range. For higher secondary energies, bremsstrahlung and photonuclear interactions are the dominant effects. Another effect that can be seen is the energy cut at $e_{\text{cut}} = 500 \text{ MeV}$ where the histogram cuts off abruptly. The energy losses below e_{cut} correspond to losses where $E \cdot v < e_{\text{cut}}$ but $v > v_{\text{cut}} = 0.05$. These losses are dominated by ionization losses since ionization is the relevant process for low energies.

The two-dimensional histograms in figure 2.4 show the sorted energy losses correlated with the energy of the initial particle at the time of the interaction. Here, 10^3 muons

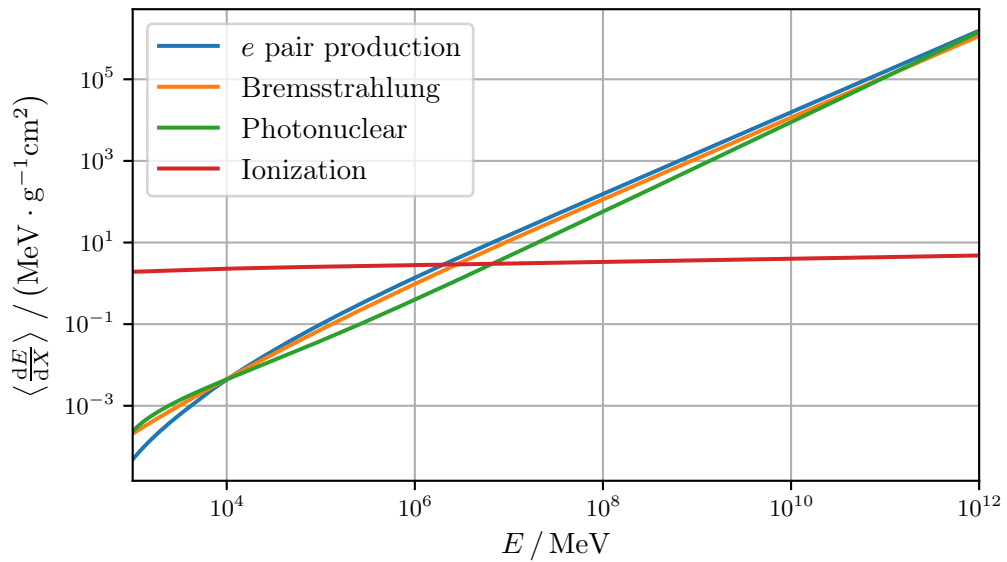


Figure 2.2: Continuous energy losses of muons in ice. No energy cuts are applied in this plot, hence this plot represents the case where all losses are treated continuous.

with an initial energy of 10^{14} MeV are propagated. Table 2.1 additionally shows the sum of the secondary energy losses as well as the frequency of the energy losses for every possible interaction.

It can be seen that bremsstrahlung and photonuclear interaction tend to have a more homogeneous spectrum where the secondary energy is less correlated with the primary energy than for ionization and pair production. For bremsstrahlung, the effects of the LPM effect can be seen since this effect causes the bremsstrahlung cross section to be suppressed for small v at very high energies. Especially for the ionization histogram the effects of the combined e_{cut} and v_{cut} can be seen for small primary energies leading to secondary energies below e_{cut} . Table 2.1 shows that the sum of the energy losses are of the same order of magnitude for pair production, bremsstrahlung and photonuclear interaction while the contribution for ionization is significantly lower since the latter is mainly treated continuously. Although the energy loss contribution of pair production is comparable to bremsstrahlung and photonuclear interaction its frequency is of several orders of magnitude higher due to its tendency to produce energy losses with a smaller relative energy.

Adapt numbers
in captions of
figures

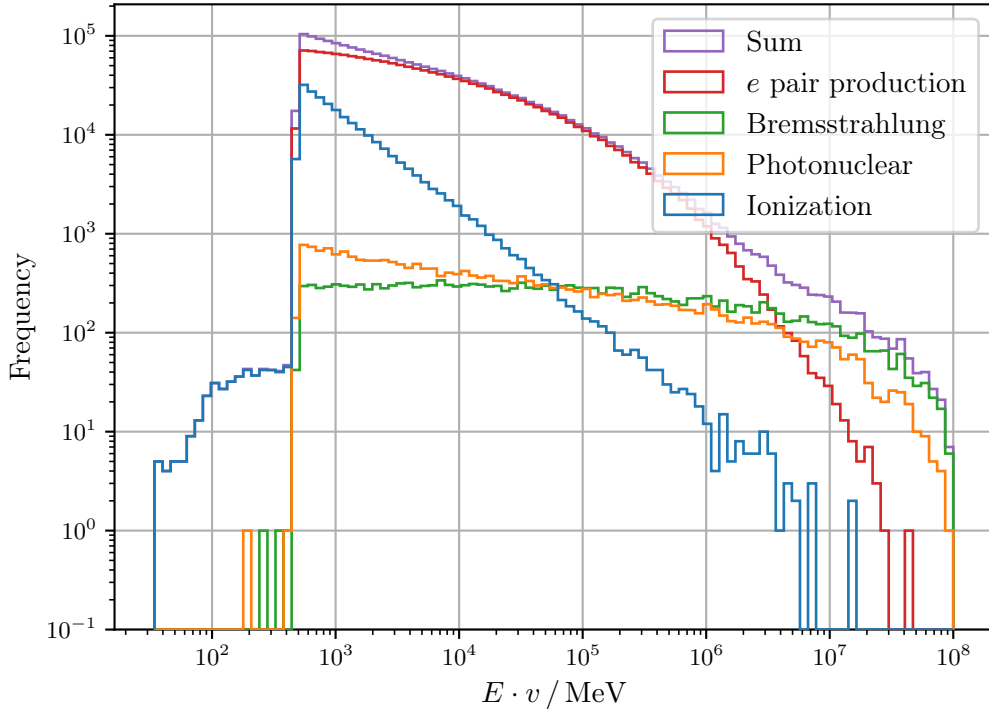


Figure 2.3: Secondary particle spectrum for 10^5 muons with an initial energy of 10^8 MeV, propagated in ice. The histogram shows the frequency of the stochastic losses during propagation, classified by the type of energy loss. The energy cuts applied here are $e_{\text{cut}} = 500$ MeV, $v_{\text{cut}} = 0.05$.

Table 2.1: Interaction-specific frequency and sum of stochastic energy losses according to figure 2.4.

Interaction	Frequency	$\sum E_{\text{prim}} \cdot v / \text{MeV}$
pair production	2.68e+7	2.99e+16
Bremsstrahlung	7.33e+4	2.26e+16
Photonuclear	2.05e+5	4.75e+16
Ionization	7.96e+5	5.21e+9

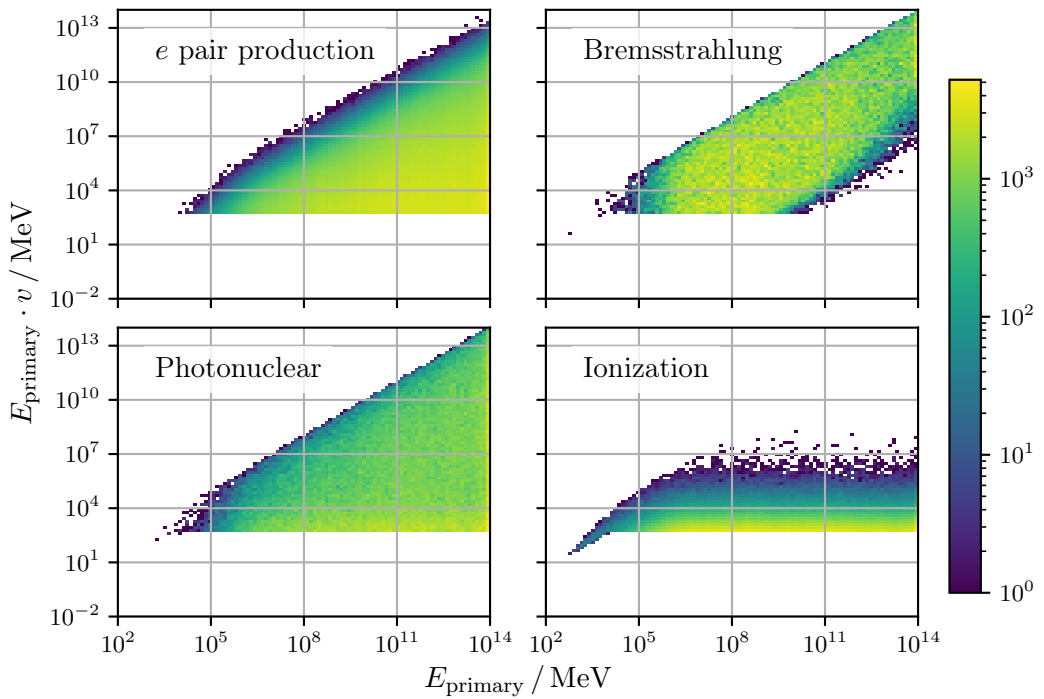


Figure 2.4: Energy spectra for 10^3 muons with an initial energy of $E = 10^{14} \text{ MeV}$ propagated in ice. For each histogram, the x-axis shows the energy of the primary particle before the stochastic loss and the y-axis the energy of the secondary particle created in the stochastic loss. The energy cuts applied here are $e_{\text{cut}} = 500 \text{ MeV}$, $v_{\text{cut}} = 0.05$.

3 Integration of rare processes

3.1 Muon pair production

The process of muon pair production is a rare process with a negligible contribution to the overall energy loss of a propagated particle. Although quantitatively negligible, the created signatures may be qualitatively relevant for neutrino observatories such as IceCube or underground detectors examining muons, see section 3.1.3 for a description of these signatures.

3.1.1 Theoretical description

Muon pair production describes the creation of a muon-antimuon pair by a particle in the field of an atomic nucleus Z , in case of an initial muon the reaction is

$$\mu^- + Z \rightarrow \mu^- + \mu^+ + \mu^- + Z.$$

A feynman diagram in leading order for the process is shown in figure 3.1.

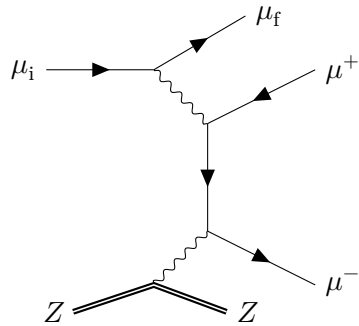


Figure 3.1: One possible feynman diagram describing the creation of a muon pair by an ingoing muon.

The process has been described in [7] where a simplified analytical double-differential cross section for muon pair production is given by

$$\frac{d^2\sigma}{dv d\rho} = \frac{2}{3\pi} (Z\alpha r_\mu)^2 \frac{1-v}{v} \Phi(v, \rho) \ln(X(E, v, \rho)) \quad (3.1)$$

with the relative energy loss v and the asymmetry parameter ρ defined by

$$v = \frac{E_+ + E_-}{E}, \quad \rho = \frac{E_+ - E_-}{E_+ + E_-} \quad (3.2)$$

and the energy of the produced (anti)muon E_+ , E_- . The functions $\Phi(v, \rho)$ and $X(E, v, \rho)$ have the form

$$\begin{aligned} \Phi(v, \rho) = & [(2 + \rho^2)(1 + \beta) + \xi(3 + \rho^2)] \cdot \ln \left(1 + \frac{1}{\xi} \right) \\ & + \left[(1 + \rho^2) \left(1 + \frac{3}{2}\beta \right) - \frac{1}{\xi}(1 + 2\beta)(1 - \rho^2) \right] \cdot \ln(1 + \xi) \\ & - 1 - 3\rho^2 + \beta(1 - 2\rho^2) \end{aligned} \quad (3.3)$$

where X is given by

$$X = 1 + U(E, v, \rho) - U(E, v, \rho_{\max}) \quad (3.4)$$

with

$$U(E, v, \rho) = \frac{\frac{0.65m_\mu}{m_e} A^{-0.27} B Z^{-1/3}}{1 + \frac{2\sqrt{e}\mu^2 B Z^{-1/3}(1+\xi)(1+Y)}{m_e E v (1-\rho^2)}} \quad (3.5)$$

and with

$$\xi = \frac{v^2(1 - \rho^2)}{4(1 - v)}, \quad \beta = \frac{v^2}{2(1 - v)}, \quad Y = 12\sqrt{\frac{m_\mu}{E}}, \quad B = 183. \quad (3.6)$$

The approximative expression (3.1) takes into account the finiteness of the nucleus as well as screening effects of the nucleus by atomic electrons. A more precise formula for the differential cross section is given in [7] as well, however it includes multidimensional integrals that are hard to evaluate and is therefore not suited to be used here. Furthermore, (3.1) is chosen to have a discrepancy compared to the precise formula of below 10 % for all $E > 10^4$ MeV, the discrepancy of the derived total cross section is even below 3 % for $E > 3 \times 10^4$ MeV.

The kinematic limits of the process for v and ρ are

$$v_{\min} = \frac{2m_\mu}{E}, \quad v_{\max} = 1 - \frac{m}{E}, \quad |\rho| \leq \rho_{\max} = 1 - \frac{2m_\mu}{vE}, \quad (3.7)$$

for an initial particle with mass m and are easy to retrace by demanding the condition that all particles involved have to fulfill $E > m_{\text{rest}}$ at all times.

3.1.2 Implementation in PROPOSAL

The process of muon pair production is implemented as an optional, additional interaction in PROPOSAL. It is per default disabled in PROPOSAL and can be enabled by setting the keyword `mupair` in the configuration file to `MupairKelnerKokoulinPetrukhin` which is the parametrization that has been described in the previous section.

To obtain the single-differential cross section in v from (3.1), a numerical integration across the entire kinematic range of ρ

$$\frac{d\sigma}{dv} = \int_{\rho_{\min}}^{\rho_{\max}} \frac{d^2\sigma}{dv d\rho} d\rho \quad (3.8)$$

is performed in PROPOSAL. After sampling the relative energy loss v during propagation according to (2.17), the asymmetry parameter ρ is also sampled if the parameter `mupair_particle_output` has been set to `True`. In this case, (3.1) is used with a fixed $v = v^*$ to solve the integral equation

$$\left(\frac{d\sigma}{dv}(v^*) \right)^{-1} \int_{\rho_{\min}}^{\rho} \frac{d^2\sigma}{dv d\rho}(v^*) d\rho = \xi \quad (3.9)$$

for ρ where $\xi \in [0, 1]$ is a random number. An additional random number is used to decide on the sign of ρ , the muon energies then assigned are $E_{\pm} = vE \cdot (1 \pm \rho)$. In figure 3.2, the behavior of ρ for different muon energies and different v is shown. For high energies, the process tends to have a higher asymmetry ρ , especially when a high relative energy loss is involved, while for lower energies, lower asymmetries are favored.

A comparison of the average energy loss in ice due to electron-positron pair production and muon pair production is shown in figure 3.3. Both functions behave similarly as they both grow linearly with E , still the contribution from muon pair production is by about three orders of magnitudes lower for higher energies and even lower for small energies. This observation shows that the process is negligible for the energy loss for the muon which is especially a result of the difference between the muon mass and the electron mass since

$$\frac{\sigma_{\mu\text{pair}}}{\sigma_{e\text{pair}}} \propto \frac{r_{\mu}^2}{r_e^2} \propto \frac{m_e^2}{m_{\mu}^2} \propto 2 \times 10^{-5}.$$

Figure 3.4 shows a secondary particle spectrum where muon pair production is enabled. The contribution for muon pair production tends to be distributed homogeneously but is, as expected, quantitatively negligible for all secondary energies.

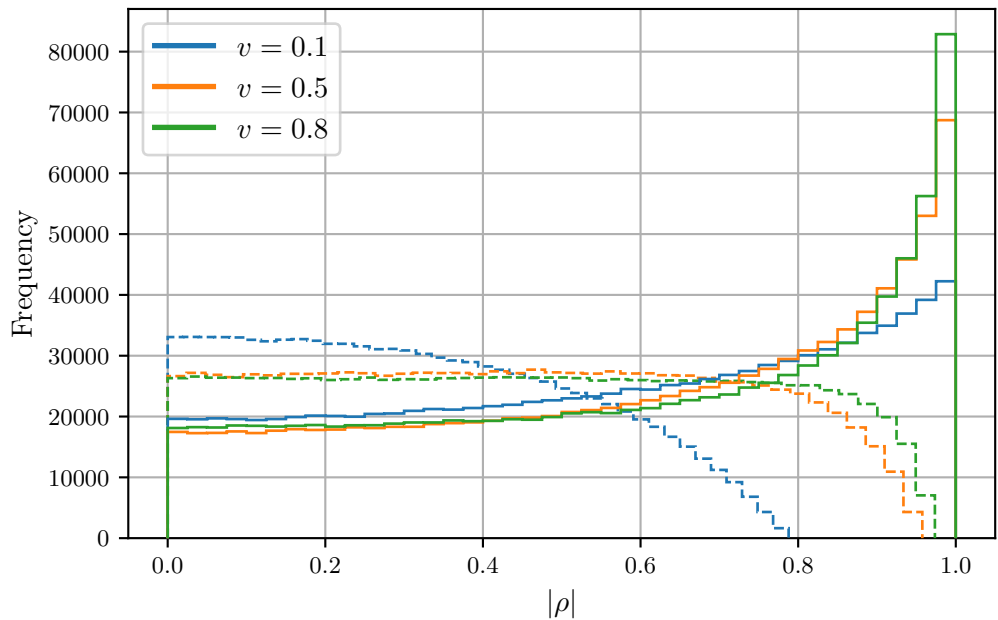


Figure 3.2: Histogram of $|\rho|$ for different v of muons in ice. For each v , ρ has been sampled 10^6 times. The dashed curves correspond to an initial muon energy of $E = 10^4$ MeV, the solid curves to $E = 10^9$ MeV.

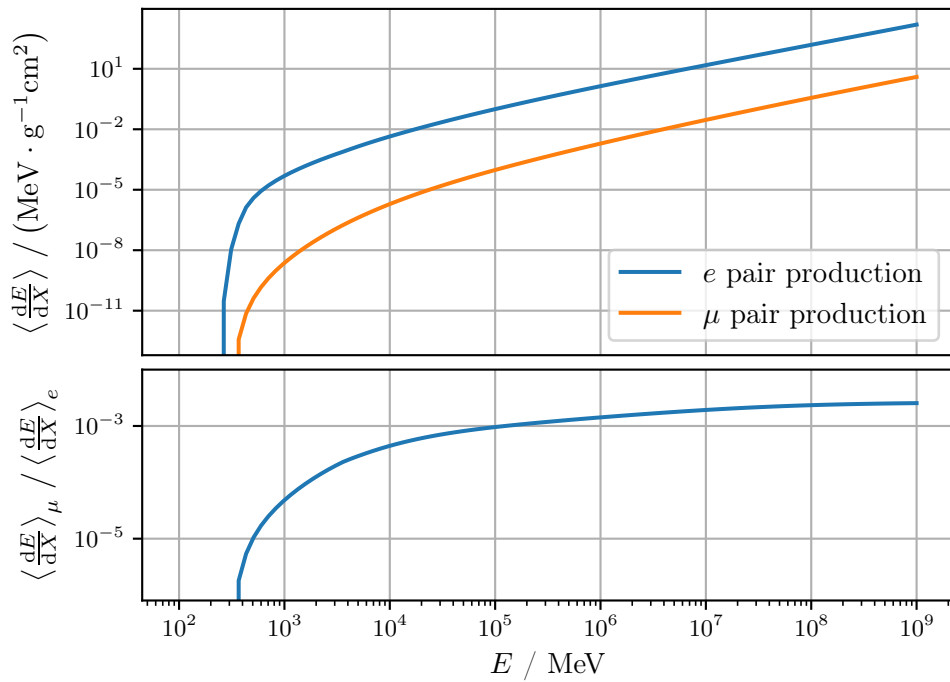


Figure 3.3: Comparison of the average continuous energy losses of muons in ice due to electron-positron pair production and muon pair production. No energy cuts are applied in this plot, hence this plot represents the case where all losses are treated continuous.

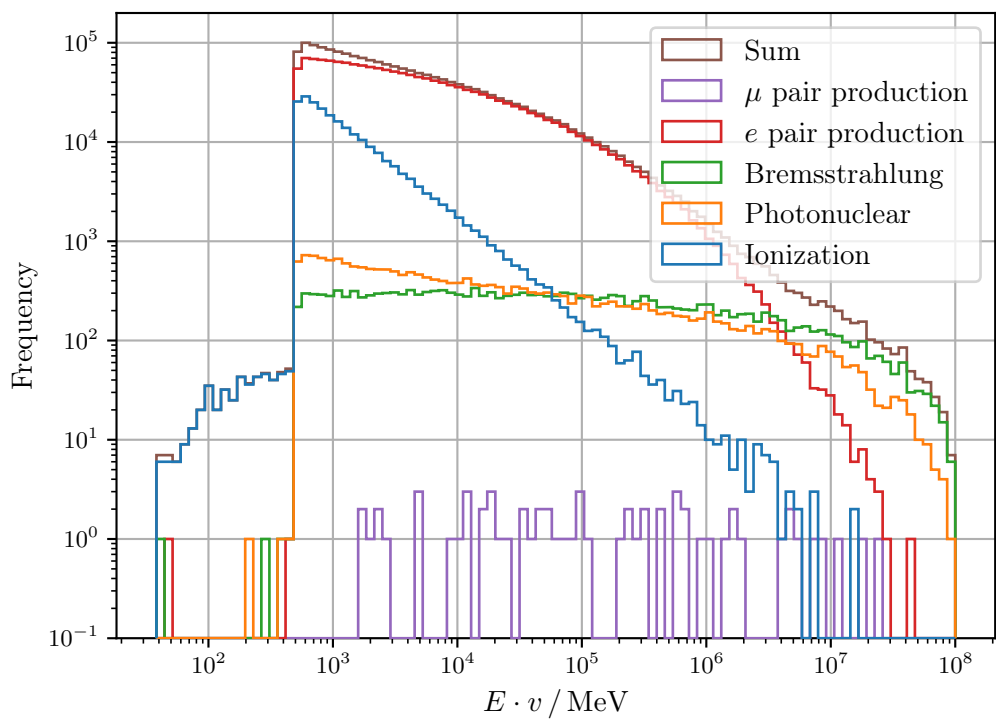


Figure 3.4: Secondary particle spectrum for 10^5 muons with an initial energy of 10^8 MeV, propagated in ice. Muon pair production is enabled. The histogram shows the frequency of the stochastic losses during propagation, classified by the type of energy loss. The energy cuts applied here are $e_{\text{cut}} = 500$ MeV, $v_{\text{cut}} = 0.05$.

3.1.3 Significant detector signatures

As already described and shown in section 3.1.2, the contribution of muon pair production to the overall energy loss of muons is negligible. However, for detectors interested in muon events, the effects of muon pair production may portray a source of significant signatures. In the following, a group of muons moving into almost the same direction with only a small separation is called a muon bundle. The origin of such a bundle can be muon pair production, in this case the bundle consists of three muons.

IceCube detector

Due to resolution effects, the IceCube detector is unable to identify the muons in a bundle as individual muon signatures. However, the signature of a single muon traversing the detector is different from a muon bundle originating from muon pair production with the same sum of energy. The signature of a high-energetic muon in IceCube is often characterized by a single high-energetic stochastic energy loss creating a spherical signature. In a muon bundle, each muon with only a fraction of the total energy produces smaller stochastic losses. Since the stochastic losses of the individual muons in the bundle are independent of each other, the resulting signature is homogeneous and the energy loss per distance of a bundle is more consistent compared to the energy loss per distance of a single muon with the same total energy.

Underground observatories

Underground detectors observing muons originating from extensive air showers can use the information about muon bundles created in these air showers to learn about the cosmic ray composition and hadronic interaction models. This is done by comparing the frequency and multiplicity of muon bundles as well as the muon separation measured in experiments with the predictions from Monte Carlo studies. In [9], the authors describe this procedure in more detail and point out a possible background from muon pair production.

Include an event signature of a high-energetic muon and a muon bundle event? See Tomasz dissertation as a comparison.

While about 1 % to 10 % of the observed muons are part of muon bundles induced in the air shower, these bundles can also be produced due to muon pair production in rock or water above the underground detector. According to calculations in [9], these bundles induced by muon pair production can portray a background of up to 10 % compared to the conventional bundles in the showers, although more exact calculations have to be performed individually for each experiment with its own geometric properties. Due to the difference in the distance between the creation and observation point of the muon bundle, both effects can be separated statistically by examining the separation distance in the bundle. The separation of muon bundles

due to muon pair production is mostly below 1 m while for muon bundles induced in air showers, only a small percentage of the muon bundles have such a small separation [9].

3.2 Weak interaction of charged leptons

The process called weak interaction in PROPOSAL refers to the conversion of a charged lepton to a neutrino under exchange of a W -boson, i.e. a charged current weak interaction. This interaction is highly suppressed compared to other processes, its signature however can be of importance, for example as a background for tau neutrino searches as described in section 3.2.3.

3.2.1 Theory and description of the data

The process of interest

$$l + N \rightarrow \nu_l + X \quad (3.10)$$

with a charged lepton l , the corresponding neutrino ν_l , the initial nucleon N and the hadronic final state X describes the conversion of a charged lepton to a neutrino under exchange of a W -boson. This specific process is related to the interaction of an anti-neutrino under exchange of a W boson, i.e.

$$\bar{\nu}_l + N \rightarrow \bar{l} + X, \quad (3.11)$$

via crossing symmetry¹ as depicted in figure 3.5. Since the kinematics of both processes are identical, the differential cross sections are also identical except for a prefactor of $1/2$,

$$d\sigma(l + N \rightarrow \nu_l + X) = \frac{1}{2} d\sigma(\bar{\nu}_l + N \rightarrow \bar{l} + X). \quad (3.12)$$

Due to averaging over all possible initial states and summing over all possible final states when evaluating feynman diagrams, the prefactor $1/2$ must be taken into account since the muon can both be left-handed and right-handed while neutrinos are only observed in a left-handed state (and antineutrinos in a right-handed state).

Data on the differential cross section for the conversion of a neutrino to a charged lepton, i.e. the process (3.11), are available from [4]. By using crossing symmetry,

¹The argument of crossing symmetry is identical when switching all particles with their corresponding antiparticles, i.e. the process $\bar{l} + N \rightarrow \bar{\nu}_l + X$ is connected to $\nu_l + N \rightarrow l + X$.

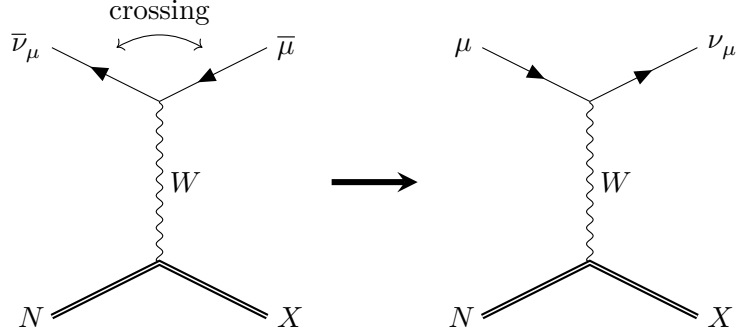


Figure 3.5: Feynman diagrams of lepton interactions under exchange of a W -boson and its connection via crossing symmetry.

these data can directly be used to describe the conversion of a charged lepton to a neutrino, i.e. (3.10), which is the process of interest in PROPOSAL.

The cross sections for interactions of leptons with hadrons can be derived under the use of parton distribution functions which describe the probability to find a specific parton (quark or gluon) with a given fraction x of the nucleon's momentum when the momentum transfer is given by Q^2 . To make predictions for the (anti)neutrino charged current cross sections, [4] performs next-to-leading order calculations and uses the HERAPDF1.5 data set which provides the parton distribution functions based on deep-inelastic scattering measurements performed from 2003 to 2007 at the HERA experiment [3].

The values for $d\sigma/dv$ are provided as two-dimensional tables in E and v with 100 entries in E and, for each energy, 110 entries in v . Here, v describes the fraction of the initial lepton energy E lost to the nucleon. Tables are available for an ingoing neutrino or an ingoing antineutrino and for a proton or a neutron as a nucleon involved in the interaction. The ranges are $10 \text{ GeV} \leq E \leq 10^{12} \text{ GeV}$ and $v_{\min} < v < 1$ with logarithmic steps in between where the lower limit of v has been set to

$$v_{\min} = \frac{Q_{\min}^2}{s}, \quad s = 2Em + m^2, \quad Q_{\min}^2 = 1 \text{ GeV}^2 \quad (3.13)$$

with the mass of the involved nucleon m and the center-of-mass energy \sqrt{s} . For values where $Q^2 < Q_{\min}^2$, the underlying theory of quantum chromodynamics can not be treated perturbatively anymore, meaning that the predictions for the cross sections are not reliable in this kinematic range.

3.2.2 Implementation in PROPOSAL

The weak interaction process is by default disabled in PROPOSAL and can optionally be enabled by setting the keyword `weak` in the configuration file to `CooperSarkarMertsch` which is the parametrization described in the previous section.

For a component with an atomic number Z and a mass number A , the differential cross section is combined from the given tables to be

$$\frac{d\sigma}{dv} \propto Z \cdot \frac{d\sigma_p}{dv} + (A - Z) \cdot \frac{d\sigma_n}{dv} \quad (3.14)$$

where the subscript refers to the nucleon involved in the interaction (p for proton and n for neutron). PROPOSAL then uses a two-dimensional interpolation routine to obtain a continuous differential cross section from the discrete tables values.

In contrast to previously described processes, the weak interaction is a catastrophic loss meaning that the initial particle ceases to exist since it is converted to a different type of particle during the interaction. Treating a process with this signature continuously as described in section 2.1.1 would therefore be unphysical. Instead, all interactions with catastrophic losses are treated stochastically by setting $v_{\min} = v_{\text{cut}}$ in (2.5), (2.16) and (2.17). Afterwards, PROPOSAL returns the produced neutrino as well as the energy transfer to the nucleon and stops the particle propagation.

Figure 3.6 shows the weak interaction cross section of muons in ice compared to the total stochastic cross section of default processes. It is important to note for this comparison that, while $v_{\min} = v_{\text{cut}}$ is used for the weak interaction, a regular energy cut of $e_{\text{cut}} = 500$ MeV and $v_{\text{cut}} = 0.05$ is still used for the other parametrizations. Still, it becomes obvious that the weak interaction is a strongly suppressed process compared to all other interactions.

3.2.3 Significant detector signatures

As described in the previous section, the weak interaction process is highly suppressed and therefore negligible in its contribution to the energy loss of a charged lepton. However, under certain conditions, the detector signature of the process could be significant for searches of tau neutrinos, for example in the IceCube neutrino observatory.

One possible signature hinting at a tau neutrino event called the "lollipop" signature is illustrated in figure 3.7a. Here, a tau neutrino moving towards the detector interacts via a charged current before it reaches the detector and is being converted

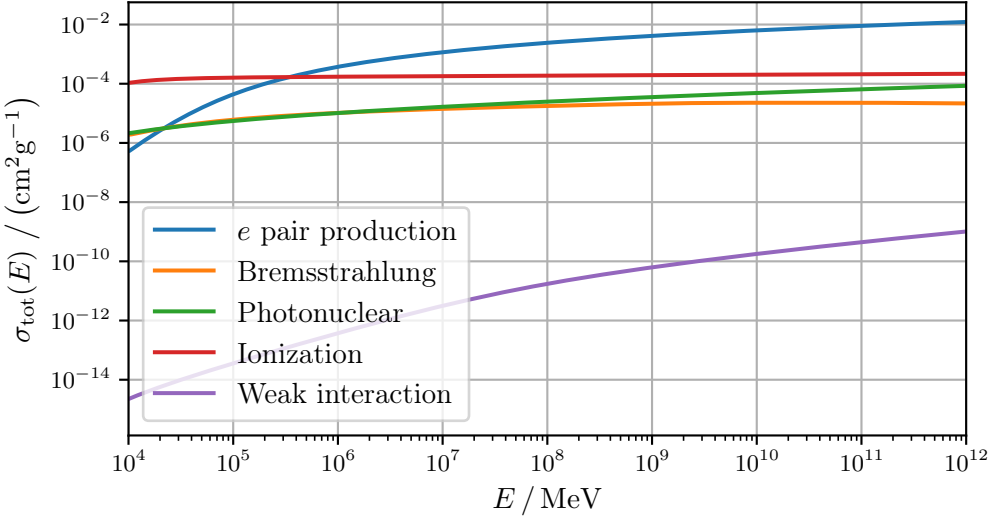


Figure 3.6: Comparison of the stochastic cross sections for muons in ice for weak interaction in comparison to other interactions. The cut settings are set to $e_{\text{cut}} = 500 \text{ MeV}$, $v_{\text{cut}} = 0.05$. Note that the weak interaction cross section is not affected by the cut settings.



(a) Lollipop signature triggered by a tau neutrino.

(b) Signature of a muon weakly interacting inside the detector.

Figure 3.7: Illustrations of two signatures relevant for tau neutrino searches. The detector volume is drawn gray, hadronic cascades are drawn as a red dot, observable tracks are drawn as blue lines and tracks that are not directly observable are drawn as a black, dotted line.

to a tau lepton. The tau lepton then enters the detector, leaving behind an observable track of Cherenkov light emerging from the tau itself and the created secondary particles. Due to its short lifetime, the created tau can only reach the detector if its energy is high enough, the average tau decay length scales with energy as 5 cm/TeV [1] meaning the tau energy has to be $E_\tau \gtrapprox 100 \text{ TeV}$. If the tau decays to a hadron inside the detector, a hadronic cascade is generated at the end of the track, giving the signature its characteristic name.

This tau neutrino signature can be imitated by the event shown in figure 3.7b. In this case, a muon, leaving behind a track, enters the detector where it weakly interacts and is therefore converted to a neutrino. Due to the energy transfer to the involved nucleus in the weak interaction, the process creates a hadronic cascade comparable to the cascade of a hadronic tau decay. Since the created neutrino is not observable, the overall signature where a track starts outside the detector and ends in a hadronic cascade can be confused with the lollipop signature from figure 3.7a. However, the tracks from both signatures behave differently since the energy loss per distance of a muon is higher than the energy loss of a tau. To have a similar track signature, the tau involved needs to have an energy that is about 6 to 11 times higher than the energy of a corresponding muon [10].

It follows that analyses searching for lollipop signatures have to consider the weak interaction as a possible background. According to approximative calculations in [10] based on the properties of the IceCube detector, the expected rate of false lollipop events due to atmospheric muons undergoing weak interaction is about $2 \times 10^{-2} / \text{yr}$. This, together with further approximative calculations for real lollipop signatures from tau neutrino events, corresponds to a possible background of 10 %. However, further effects such as event selection efficiency (assumed to be perfect in this calculation) or a detailed detector simulation were not taken into account but need to be evaluated when conducting a detailed analysis.

4 Propagation of electromagnetic showers

A Anhang

Bibliography

- [1] M. G. Aartsen et al. “Search for astrophysical tau neutrinos in three years of IceCube data”. In: *Physical Review D* 93.2 (Jan. 2016). ISSN: 2470-0029. DOI: 10.1103/physrevd.93.022001. URL: <http://dx.doi.org/10.1103/PhysRevD.93.022001>.
- [2] Dmitry Chirkin and Wolfgang Rhode. *Propagating leptons through matter with Muon Monte Carlo (MMC)*. 2004. arXiv: hep-ph/0407075 [hep-ph].
- [3] Amanda Cooper-Sarkar. *Proton Structure from HERA to LHC*. 2010. arXiv: 1012.1438 [hep-ph].
- [4] Amanda Cooper-Sarkar, Philipp Mertsch, and Subir Sarkar. “The high energy neutrino cross-section in the Standard Model and its uncertainty”. In: *Journal of High Energy Physics* 2011.8 (Aug. 2011). ISSN: 1029-8479. DOI: 10.1007/jhep08(2011)042. URL: [http://dx.doi.org/10.1007/JHEP08\(2011\)042](http://dx.doi.org/10.1007/JHEP08(2011)042).
- [5] Mario Dunsch et al. *Recent Improvements for the Lepton Propagator PROPOSAL*. 2018. DOI: 10.1016/j.cpc.2019.03.021. arXiv: 1809.07740 [hep-ph].
- [6] Malte Geisel-Brinck. “Revision of the multiple scattering algorithms in PROPOSAL”. In: 2013.
- [7] S. R. Kel’ner, R. P. Kokoulin, and A. A. Petrukhin. “Direct production of muon pairs by high-energy muons”. In: *Physics of Atomic Nuclei* 63.9 (Sept. 2000), pp. 1603–1611. ISSN: 1562-692X. DOI: 10.1134/1.1312894. URL: <https://doi.org/10.1134/1.1312894>.
- [8] Jan-Hendrik Köhne. “Der Leptonpropagator PROPOSAL”. PhD thesis. Tech. U., Dortmund (main), 2013. DOI: 10.17877/DE290R-13191. URL: <http://hdl.handle.net/2003/32866>.
- [9] V.A. Kudryavtsev, E.V. Korolkova, and N.J.C. Spooner. “Narrow muon bundles from muon pair production in rock”. In: *Physics Letters B* 471.2 (1999), pp. 251–256. ISSN: 0370-2693. DOI: [https://doi.org/10.1016/S0370-2693\(99\)01378-7](https://doi.org/10.1016/S0370-2693(99)01378-7). URL: <http://www.sciencedirect.com/science/article/pii/S0370269399013787>.

Bibliography

- [10] Alexander Sandrock. “Higher-order corrections to the energy loss cross sections of high-energy muons”. PhD thesis. Tech. U., Dortmund (main), 2018. doi: [10.17877/DE290R-19810](https://doi.org/10.17877/DE290R-19810).
- [11] M. Tanabashi et al. “Review of Particle Physics”. In: *Phys. Rev. D* 98 (3 Aug. 2018), p. 030001. doi: [10.1103/PhysRevD.98.030001](https://doi.org/10.1103/PhysRevD.98.030001). URL: <https://link.aps.org/doi/10.1103/PhysRevD.98.030001>.

Eidesstattliche Versicherung

Ich versichere hiermit an Eides statt, dass ich die vorliegende Abschlussarbeit mit dem Titel "Working title" selbstständig und ohne unzulässige fremde Hilfe erbracht habe. Ich habe keine anderen als die angegebenen Quellen und Hilfsmittel benutzt, sowie wörtliche und sinngemäße Zitate kenntlich gemacht. Die Arbeit hat in gleicher oder ähnlicher Form noch keiner Prüfungsbehörde vorgelegen.

Ort, Datum

Unterschrift

Belehrung

Wer vorsätzlich gegen eine die Täuschung über Prüfungsleistungen betreffende Regelung einer Hochschulprüfungsordnung verstößt, handelt ordnungswidrig. Die Ordnungswidrigkeit kann mit einer Geldbuße von bis zu 50 000 € geahndet werden. Zuständige Verwaltungsbehörde für die Verfolgung und Ahndung von Ordnungswidrigkeiten ist der Kanzler/die Kanzlerin der Technischen Universität Dortmund. Im Falle eines mehrfachen oder sonstigen schwerwiegenden Täuschungsversuches kann der Prüfling zudem exmatrikuliert werden (§ 63 Abs. 5 Hochschulgesetz –HG–).

Die Abgabe einer falschen Versicherung an Eides statt wird mit Freiheitsstrafe bis zu 3 Jahren oder mit Geldstrafe bestraft.

Die Technische Universität Dortmund wird ggf. elektronische Vergleichswerkzeuge (wie z. B. die Software "turnitin") zur Überprüfung von Ordnungswidrigkeiten in Prüfungsverfahren nutzen.

Die oben stehende Belehrung habe ich zur Kenntnis genommen.

Ort, Datum

Unterschrift